Journal of Materials Chemistry B

ROYAL SOCIETY OF CHEMISTRY

PAPER

View Article Online
View Journal | View Issue

Cite this: J. Mater. Chem. B, 2024, 12, 2413

Water-soluble red fluorescent protein dimers for hypoxic two-photon photodynamic therapy†

Wan Feng and Ying Qian *

In this study, two water-soluble red fluorescent protein (RFP) dimers, FP_2R' and FP_2R'', were synthesized by linking two phenothiazine-based RFP chromophore analogues through alkyl chains or alkoxy chains for hypoxic two-photon photodynamic therapy. RFP dimers are heavy-atom-free two-photon photosensitizers in which the intersystem crossing process is boosted by S and N heteroatoms. In terms of the aqueous solubility, the saturation concentration of FP_2R'' was 3.5 mM, the emission wavelength was 677 nm, the singlet oxygen yield was 18%, and the two-photon absorption coefficient (β) was 2.1×10^{-11} cm W^{-1}. Further, the RFP dimer FP_2R'' showed excellent biocompatibility, negligible dark toxicity, and could produce $^1O_2$ and $O_2^{\bullet-}$ simultaneously. Under 460 nm illumination, the photosensitizer FP_2R'' showed high phototoxicity with an IC_{50} value of 4.08 μM in an hypoxia environment, indicating that the photosensitizer FP_2R'' has an excellent anti-hypoxia ability. In addition, the photosensitizer FP_2R'' demonstrated a precise localization ability to lysosomes and its Pearson's colocalization coefficient was 0.94, which could guide the aggregation of photosensitizers in the lysosomes of tumor cells to effectively improve its photodynamic therapy (PDT) effect. In particular, when exposed to 800 nm two-photon excitation, FP_2R'' effectively produced $^1O_2$ and $O_2^{\bullet-}$ in zebrafish and exhibited a bright two-photon fluorescence imaging capability. At the same time, the efficacy of two-photon photodynamic therapy mediated by the photosensitizer FP_2R'' was verified in the tumor zebrafish model, and the growth of tumor cells in zebrafish was significantly inhibited under a two-photon laser irradiation. The water-soluble two-photon photosensitizer FP_2R'' that was reasonably constructed in this study can be used as a high-efficiency hypoxic two-photon photosensitizer to inhibit deep tumor tissues.

Received 6th November 2023,
Accepted 30th January 2024

DOI: 10.1039/d3tb02621c

rsc.li/materials-b

1. Introduction

Hypoxia-dependent photosensitizers are the preferred choice for treating solid tumors. However, the limitations of poor water solubility, a short emission wavelength, low biocompatibility, and the inability to distinguish cancer cells from normal cells have constrained the clinical application of most photosensitizers.[1–5] In recent years, researchers have primarily focused on enhancing the water solubility of photosensitizers by encapsulating them in amphiphilic polymers and proteins to form nanoparticles.[6–10] Nevertheless, the tight encapsulation of nanoparticles not only leads to insufficient internal oxygen but also impedes the diffusion of ROS, resulting in reduced efficacy.[11–13] While the introduction of multiple quaternary ammonium salts or sulfonates into the molecule has proven effective in improving the water solubility of photosensitizers, issues such as the complex synthesis steps involved and difficult separation persist. Therefore, the development of a straightforward method to obtain highly water-soluble hypoxic photosensitizers would hold significant importance in the realms of cancer diagnosis and treatment.

Green fluorescent protein is a natural substance derived from jellyfish, and its central fluorescent chromophore, *p*-hydroxybenzylidene-2,3-dimethylimidazolinone (HBI), exhibits excellent biocompatibility. Moreover, such chromophores possess a large Stokes shift, good water solubility, and outstanding photophysical properties.[14–18] Consequently, they find widespread application in fluorescence imaging and as biological probes.[19–23] Despite their success in these areas, the exploration and reporting of fluorescent protein (FP) chromophore analogues in the field of photodynamic therapy (PDT) remain limited.[24–29] Existing FP chromophore analogues tend to be hydrophobic, constraining their further development in the biological domain. Therefore, it would be of significant importance to modify the structure of FP chromophore analogues to address the aforementioned challenges.

According to studies reported by our research group, phenothiazine-based FP chromophore analogues can effectively promote the production of $^1O_2$ and have excellent biocompatibility.[30–33]

School of Chemistry and Chemical Engineering, Southeast University, Nanjing, 211189, China. E-mail: yingqian@seu.edu.cn

† Electronic supplementary information (ESI) available. See DOI: https://doi.org/10.1039/d3tb02621c

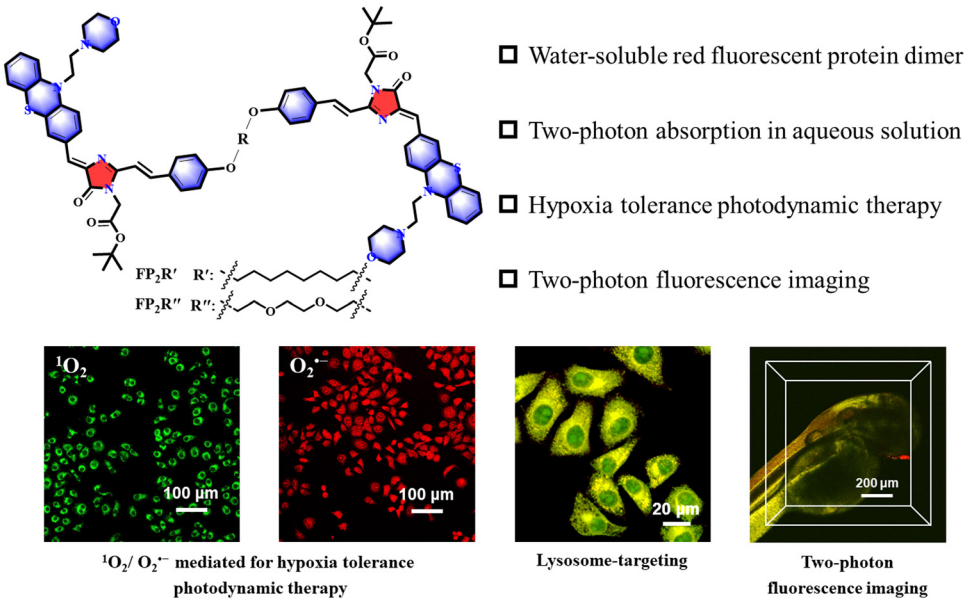

Scheme 1 Structures of the water-soluble and heavy-atom-free RFP dimers FP_2R' and FP_2R'' and their application in two-photon photodynamic therapy.

Based on the above inspiration, two heavy-atom-free RFP dimers (FP_2R' and FP_2R'') were synthesized to solve the poor aqueous solubility and hypoxia problem. As shown in Scheme 1, the aqueous solubility of the RFP dimer FP_2R'' was significantly improved by the alkoxy chain-linked. This article studies the influence of the alkyl chain-links and alkoxy chain-links through UV-vis absorption, fluorescence emission spectroscopy, and the Z-scan technique as well as explains the mechanism of ROS generation through theoretical calculations. Intracellular PDT experiments and lysosome-targeting experiments were used to evaluate the potential of FP_2R'' as an hypoxic photosensitizer in the biological field. Under 800 nm two-photon excitation, the effective ROS production of FP_2R'' was investigated in zebrafish. The results confirmed that the heavy-atom-free alkoxy chain-linked RFP dimer FP_2R'' could be used as a candidate for hypoxic two-photon photosensitizers and could be expected to be applied in the treatment of hypoxic tumor cells.

2. Experimental section

2.1 Materials and methods

The synthetic routes of the RFP chromophore analogues FPOH, FP_2R', and FP_2R'' are presented in Scheme 2. The detailed description and illustration of the intermediates and target photosensitizers are provided in the ESI† (Fig. S10–S27). High-resolution mass spectroscopy (HRMS), and ^{1}H NMR and ^{13}C NMR spectroscopy were used to confirm all three RFP chromophore analogues. Except when otherwise noted, all additional starting ingredients were obtained from commercial sources. All the biomaterials were purchased from Keygen Biotech Co. Ltd. A-549 cells were used in this work and were supplied by the American Type Culture Collection. Notes: N_2: nitrogen; MB: methylbenzene; EA: ethyl acetate; DCM: dichloromethane; AC: acetone; DMSO: dimethyl sulfoxide; ACN: acetonitrile.

2.2 Synthesis and characterizations

Synthesis of FPOH. Under a N_2 atmosphere, PFP-lyso (178 mg, 0.33 mmol), *p*-hydroxybenzaldehyde (101 mg, 0.83 mmol), acetic acid (113 mg, 1.33 mmol), and piperidine (78 mg, 1.33 mmol) were dissolved in 25 mL toluene. The reaction mixture was stirred at 110 °C for 6 h. The mixture was concentrated by rotary evaporation to remove the solvents after cooling to room temperature. The crude product was purified through column chromatography, yielding FPOH as a red solid (yield: 43%). ^{1}H NMR (600 MHz, DMSO-d_6, ppm): δ 10.08 (s, 1H), 8.17 (d, J = 8.4 Hz, 1H), 8.09 (s, 1H), 7.91 (d, J = 15.6 Hz, 1H), 7.69 (d, J = 8.6 Hz, 2H), 7.26–7.19 (m, 1H), 7.19–7.10 (m, 3H), 7.02–6.96 (m, 2H), 6.93 (d, J = 21.4 Hz, 1H), 6.86 (d, J = 8.6 Hz, 2H), 4.59 (s, 2H), 4.07 (t, J = 6.6 Hz, 2H), 3.63–3.54 (m, 4H), 2.69 (t, J = 6.6 Hz, 2H), 2.56–2.40 (m, 4H), 1.41 (s, 9H). ^{13}C NMR (151 MHz, DMSO, ppm): δ 170.46, 169.72, 167.34, 159.93, 159.25, 145.91, 143.53, 140.50, 137.66, 132.45, 130.51, 130.23, 129.24, 127.99, 127.27, 126.46, 123.56, 123.33, 123.06, 122.58, 116.26, 116.03, 115.88, 110.11, 82.06, 66.35, 59.88, 55.36, 53.56, 45.66, 41.99, 27.75. HRMS (*m*/*z*): $[M + H]^+$ calc. for $C_{36}H_{38}N_4O_5S$: 639.26656, found 639.25965.

Synthesis of FP_2R'. Under a N_2 atmosphere, FPOH (250 mg, 0.31 mmol), 1,8-diiodooctane (42 mg, 0.12 mmol), and K_2CO_3 (128 mg, 0.93 mmol) were dissolved in 35 mL ACN solution. The reaction mixture was stirred at 60 °C for 5 h. The mixture was concentrated by rotary evaporation to remove the solvents after cooling to room temperature. The crude product was purified through column chromatography to yield FP_2R' as a red solid (yield: 85%). ^{1}H NMR (600 MHz, $CDCl_3$, ppm): δ 8.09–8.03 (m, 3H), 8.03–7.98 (m, 3H), 7.55 (d, J = 8.7 Hz, 4H), 7.15 (td, J = 9.0, 1.2 Hz, 4H), 7.01 (s, 2H), 6.95 (t, J = 8.8 Hz, 10H), 6.48

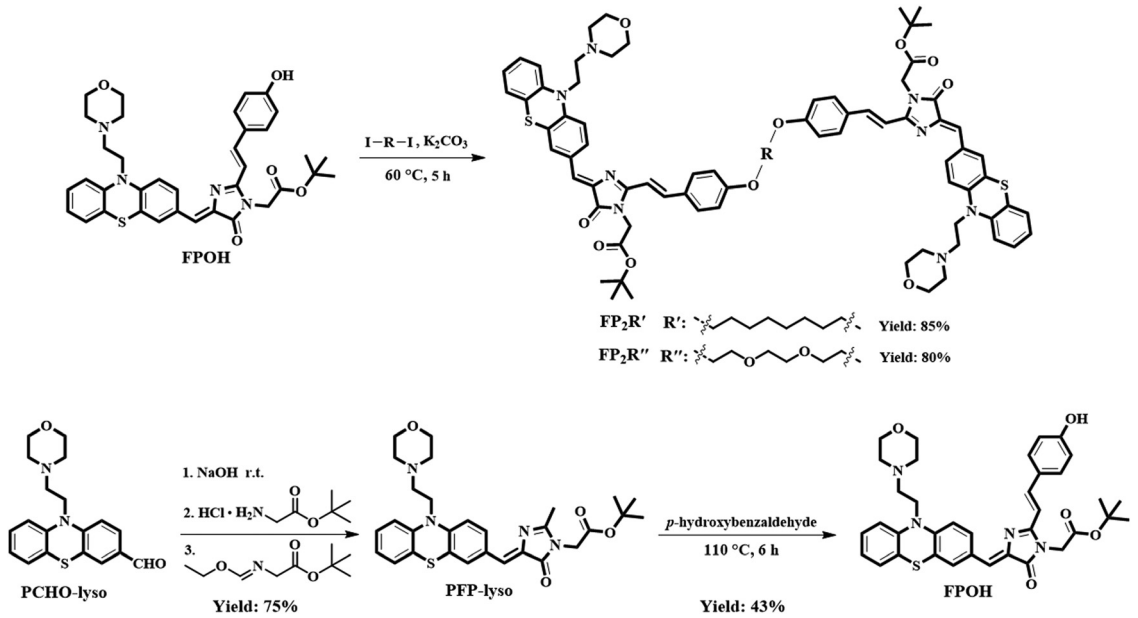

Scheme 2 Structure and synthetic route for the water-soluble red fluorescence protein chromophore analogues.

(d, J = 15.7 Hz, 2H), 4.42 (s, 4H), 4.08 (s, 4H), 4.02 (t, J = 6.5 Hz, 4H), 3.75 (s, 8H), 2.82 (s, 4H), 2.58 (s, 8H), 1.89–1.78 (m, 4H), 1.50 (s, 4H), 1.45 (s, 18H), 1.42 (s, 4H). ^{13}C NMR (151 MHz, $CDCl_3$, ppm): δ 170.19, 166.80, 161.01, 158.28, 146.26, 143.84, 140.65, 137.70, 132.36, 130.94, 129.67, 127.81, 127.55, 127.48, 125.88, 123.25, 115.55, 115.22, 114.98, 109.98, 83.10, 68.15, 66.88, 55.75, 53.91, 53.47, 42.32, 29.33, 29.19, 27.98, 26.00. HRMS (m/z): $[M + H]^+$ calc. for $C_{80}H_{90}N_8O_{10}S_2$: 1388.62915, found 1388.62884.

Synthesis of FP_2R''. Under a N_2 atmosphere, FPOH (250 mg, 0.31 mmol), 1,2-bis-(2-iodoethoxy)-ethane (44 mg, 0.12 mmol), and K_2CO_3 (128 mg, 0.93 mmol) were dissolved in 35 mL ACN solution. The reaction mixture was stirred at 60 °C for 5 h. The mixture was concentrated by rotary evaporation to remove the solvents after cooling to room temperature. The crude product was purified through column chromatography to yield FP_2R'' as a red solid (yield: 80%). ^{1}H NMR (600 MHz, $CDCl_3$, ppm): δ 8.05 (s, J = 1.4 Hz, 2H), 8.01 (s, 1H), 7.98 (d, J = 8.4 Hz, 3H), 7.54 (d, J = 8.7 Hz, 4H), 7.19–7.08 (m, 4H), 7.00 (s, 2H), 6.98–6.86 (m, 10H), 6.48 (d, J = 15.7 Hz, 2H), 4.41 (s, 4H), 4.24–4.15 (m, 4H), 4.07 (s, 4H), 3.93–3.84 (m, 4H), 3.78 (s, 4H), 3.75 (s, 8H), 2.80 (s, 4H), 2.57 (s, 8H), 1.45 (s, 18H). ^{13}C NMR (151 MHz, $CDCl_3$, ppm): δ 170.18, 166.83, 160.63, 158.24, 146.28, 143.85, 140.47, 137.73, 132.41, 130.96, 129.64, 129.58, 128.27, 127.56, 127.49, 125.96, 124.58, 124.17, 123.26, 115.58, 115.22, 115.16, 110.40, 83.09, 71.00, 69.76, 67.64, 66.87, 60.43, 55.76, 53.91, 42.36, 28.01. HRMS (m/z): $[M + H]^+$ calc. for $C_{78}H_{86}N_8O_{12}S_2$: 1392.58368, found 1392.58737.

2.3 Two-photon absorption coefficient in aqueous solution

The aqueous solutions of the RFP chromophore analogues FPOH, FP_2R', and FP_2R'' (c: 1.0 × 10^{-3} M) were, respectively, placed in a 2 mm quartz cuvette for two-photon absorption cross-section measurements. These compounds were stable toward air and laser light under the experimental conditions. The two-photon absorption and refraction were investigated with a linear polarized laser light (λ_{ex}: 800 nm; pulse width: 21 ps; repetition rate: 10 Hz; 180 fs) generated from a frequency-doubled, mode-locked, Q-switched Nd:YAG laser. The other experimental conditions for these NLO measurements were the same as described in previous reported articles.[34,35]

2.4 Detection of the $O_2^{\bullet-}$-generation ability in aqueous solution

The probe dihydrorhodamine 123 (DHR 123), which could convert the $O_2^{\bullet-}$ produced in the solution into rhodamine 123 and emit strong green fluorescence at 424 nm, was used to detect $O_2^{\bullet-}$ in the solution. The corresponding mechanism diagram is shown in Fig. S1 (ESI†). The RFP analogues FPOH, FP_2R', and FP_2R'' (10 μM) were mixed with DHR 123 (20 μM), respectively, in cuvettes. The fluorescence intensity of the mixture at 424 nm (λ_{ex} = 500 nm) were measured every 15 s under blue LED light irradiation (460 nm, 23 mW cm^{-2}).

2.5 Detection of $^1O_2$ and $O_2^{\bullet-}$ production by electron paramagnetic resonance

Detection of $^1O_2$ formation by EPR. The electron paramagnetic resonance (EPR) assay was carried out with a Bruker Magnettech ESR5000 spectroscopy system using 4-amino-2,2,6,6-tetramethylpiperidine (TEMP) as a spin-trap agent. The photosensitizers FPOH, FP_2R', and FP_2R'' were dissolved in 100 μL H_2O with a concentration of 2 × 10^{-3} M, respectively, and then 5 μL TEMP was added to the above three mixed solutions, respectively, without and with irradiation for 10 min

(460 nm, 23 mW cm^{-2}). Finally, the EPR signal was recorded at room temperature.

Detection of $O_2^{\bullet-}$ formation by EPR. The EPR assay was carried out with a Bruker Magnettech ESR5000 spectroscopy system using 5,5-dimethyl-1-pyrroline N-oxide (DMPO) as a spin-trap agent. The photosensitizers FPOH, FP_2R', and FP_2R'' were dissolved in 100 μL DMSO with a concentration of 2×10^{-3} M, respectively, an then 5 μL DMPO was added to the above three mixed solutions, respectively, without and with irradiation for 10 min (460 nm, 23 mW cm^{-2}). Finally, the EPR signal was recorded at room temperature.

2.6 Intracellular $^1O_2$ and $O_2^{\bullet-}$ production under normoxia and hypoxia in A-549 cells

Hypoxic microenvironment (2% O_2). A-549 cells were incubated with 2 μM photosensitizer FP_2R'' for 2 h under an hypoxic microenvironment and then washed twice with PBS to replace the new cell culture medium, and then 2 μM 2′,7′-dichlorodihydrofluorescein diacetate (DCFH-DA) and dihydroethidium (DHE) were added, respectively, to the cell culture dish and the cells were incubated for 15 minutes under the hypoxic microenvironment. One/two-photon fluorescence imaging was performed by one-photon confocal laser scanning microscopy (CLSM)/two-photon confocal laser scanning microscopy (TPFM).

Normoxia microenvironment (21% O_2). A-549 cells were incubated with the photosensitizer FP_2R'' (2 μM) for 2 h under a normoxia microenvironment and then washed twice with PBS to replace the new cell culture medium, and then 2 μM 2′,7′-dichlorodihydrofluorescein diacetate (DCFH-DA) and dihydroethidium (DHE) were added, respectively, to the cell culture dish and the cells were incubated for 15 minutes under the normoxia microenvironment. One/two-photon fluorescence imaging was performed by CLSM and TPFM.

2.7 Precise lysosome-targeting experiment

A-549 cells were incubated with the photosensitizer FP_2R'' (2 μM) for 2 h and then washed twice with PBS to replace the new cell culture medium, and then Lyso-Tracker Green (100 nM) (λ_{ex} = 488 nm, λ_{em} = 500–550 nm), Hoechst 33 342 (2 μg mL^{-1}) (λ_{ex} = 405 nm and λ_{em} = 430–460 nm), and Mito-Tracker Green (100 nM) (λ_{ex} = 488 nm, λ_{em} = 500–550 nm) were added to the cell culture dish separately. Next, the cells were incubated for 25 minutes and then visualized by CLSM.

2.8 Two-photon excitation-induced $^1O_2$ and $O_2^{\bullet-}$ production in zebrafish

Zebrafish were incubated in E3 culture medium (15 mM NaCl, 0.5 mM KCl, 1 mM $MgSO_4$, 1 mM $CaCl_2$, 0.15 mM KH_2PO_4, 0.05 mM Na_2HPO_4, 0.7 mM $NaHCO_3$; pH 7.5) with FP_2R'' (2 μM) for 3 h. After removing the E3 culture medium containing the photosensitizers, the zebrafish were incubated respectively in E3 culture medium containing 2 μM DCFH-DA and 2 μM DHE for 20 minutes. Finally, two-photon fluorescence images were obtained by two-photon fluorescence microscopy (TPFM) after irradiating (800 nm, 3 mW) the treated zebrafish for 15 minutes.

2.9 Two-photon photodynamic therapy for zebrafish tumor

When the zebrafish liver tumor grew to a desired size, an intravenous microinjection of FP_2R'' was performed using a nitrogen gas injector. FP_2R'' was loaded into a glass needle (20 μm), and the injection was conducted through the zebrafish retro-orbital in a continuous mode of the gas injector. The injection amount of FP_2R'' was 6–10 nL. After 24 h of injection, the zebrafish were mounted in a cell dish and then transferred to the stage of a ZEISS microscope for two-photon photodynamic therapy. A 800 nm femtosecond laser was focused on the zebrafish liver tumor with a 20× objective lens. The output laser power on the tumor surface was about 3 mW. After two-photon photodynamic therapy treatment, the zebrafish were incubated in E3 culture medium (15 mM NaCl, 0.5 mM KCl, 1 mM $MgSO_4$, 1 mM $CaCl_2$, 0.15 mM KH_2PO_4, 0.05 mM Na_2HPO_4, 0.7 mM $NaHCO_3$; pH 7.5) for 24 h, and then the tumor size was measured by two-photon confocal microscopy (ZEISS Microscope). The tumor volume was calculated using Image-J software.

2.10 Ethical statement

All animal procedures were performed in accordance with the Guidelines for Care and Use of Laboratory Animals of Southeast University and approved by the Animal Ethics Committee of Southeast University.

3. Results and discussion

3.1 The synthesis of RFP dimers

Two heavy-atom-free water-soluble RFP dimers, namely FP_2R' and FP_2R'', were synthesized for efficient hypoxic PDT. The excellent biocompatible electron acceptor *p*-hydroxybenzylidene-2,3-dimethylimidazolinone (HBI) was used as the core scaffold and the electron donor phenothiazine and morpholine were installed for ROS generation and lysosomal localization. Meanwhile, *p*-hydroxybenzaldehyde was introduced to expand the π-conjugation through the *Knoevenagel* condensation reaction, and the RFP dimers FP_2R' and FP_2R'' were obtained by linking two *p*-hydroxybenzaldehydes using alkyl or alkoxy chains (Scheme 2). Compared with FPOH, the linking of the alkyl or alkoxy chains significantly improved the aqueous solubility of the RFP dimers, enhanced the two-photon absorption characteristics of the chromophores, and promoted ROS production. Based on the above design concept, two heavy-atom-free water-soluble lysosome-targeting RFP dimers were synthesized for hypoxic PDT. Their detailed characterization and application in PDT are discussed in the following sections.

3.2 Two-photon absorption properties of the RFP dimers in aqueous solution

The two RFP dimers exhibited good aqueous solubility and the maximum absorption peaks of the RFP chromophore

Table 1 Photophysical properties of the RFP chromophore analogues in aqueous solution

	H_2O					
	λ_{abs}/nm	ε_{max}/M^{-1} cm^{-1}	λ_{em}/nm	$\Delta\lambda$/cm^{-1}	τ/ns	β_{800nm}/cm W^{-1}
FPOH	493	5100	687	5727	0.32	0.6×10^{-11}
FP_2R'	497	10 400	676	5327	0.52	1.8×10^{-11}
FP_2R''	496	11 000	677	5390	0.62	2.1×10^{-11}

analogues FPOH, FP_2R', and FP_2R'' appeared at 493 nm (ε = 5100 M^{-1} cm^{-1}), 497 nm (ε = 10 400 M^{-1} cm^{-1}), and 496 nm (ε = 11 000 M^{-1} cm^{-1}) in the aqueous solutions, respectively (Table 1). In particular, the emission wavelength of FP_2R'' was 677 nm in aqueous solution. The RFP chromophore analogues FPOH, FP_2R', and FP_2R'' all exhibited large Stokes shifts of 5727, 5327, and 5390 cm^{-1}, respectively (Table 1), effectively achieving a good separation of excitation and emission light (Fig. 1a), indicating the potential for the RFP chromophore analogues in cell imaging. The linking of the alkyl and alkoxy chains endowed FP_2R' and FP_2R'' with good aqueous solubility. Specifically, RFP dimer FP_2R'' had the biggest the saturation concentration in aqueous solution, which could reach 3.5 mM, while the saturation concentration in aqueous solution of FP_2R'' and FPOH could reach 2.9 mM and 1.4 mM as determined by their UV-vis absorption spectra (Fig. S4, ESI†). Meanwhile, FPOH, FP_2R', and FP_2R'' in aqueous solutions had short singlet fluorescence lifetimes of 0.32 ns, 0.52 ns, and 0.62 ns, respectively (Fig. 1b). The linking of the alkyl chains or alkoxy chains not only enhanced the solubility of the RFP dimers in aqueous solution, but also improved their Stokes shift, which is beneficial for intracellular imaging and minimizes the interference of background spontaneous fluorescence and the deep tissue penetration of biomolecules.

The D–A–D structure of the RFP dimers not only prolonged the absorption and emission wavelengths, but also enhanced the two-photon absorption characteristics of the chromophores. The two-photon absorption (2PA) properties of the RFP chromophore analogues FPOH, FP_2R', and FP_2R'' were tested in aqueous solution using 800 nm, 180 fs, and 10 Hz pulsed lasers by open-aperture Z-scans. The Z-scan data are shown in Fig. 1c. It is worth noting that as the number of RFP groups increased, the two-photon absorption coefficient (β) value increased in turn. Under 800 nm two-photon excitation, the β values of FPOH, FP_2R', and FP_2R'' were 0.6×10^{-11}, 1.8×10^{-11}, and 2.1×10^{-11} cm W^{-1}, respectively, and the two-photon absorption cross-sections of FPOH, FP_2R', and FP_2R'' were 25 GM, 74 GM, and 86 GM, respectively. The above experimental data indicated that the design of RFP dimers

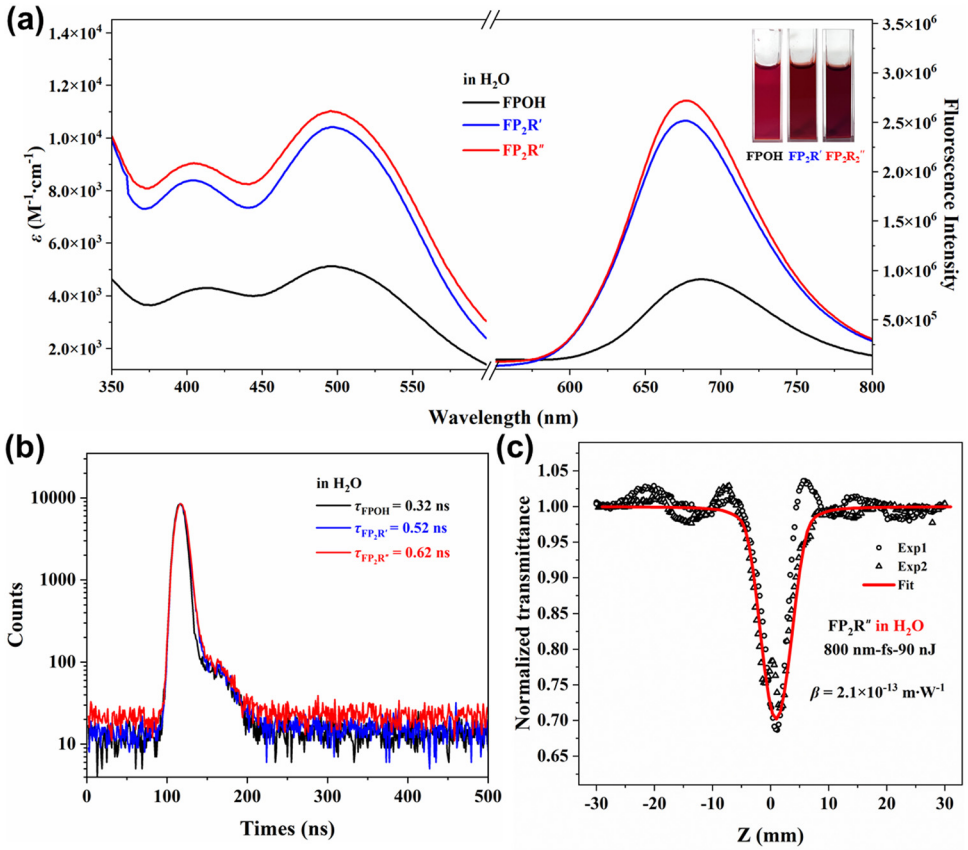

Fig. 1 (a) UV-vis absorption and fluorescence emission spectra of 10 μM of the photosensitizers FPOH, FP_2R', and FP_2R'' in aqueous solution. (b) Fluorescence lifetimes of the fluorescent protein chromophore analogues FPOH, FP_2R', and FP_2R'' in aqueous solution. (c) Normalized transmittance curves of the compound FP_2R'' under 800 nm laser irradiation.

with a D–A–D structure significantly improved the aqueous solubility of the chromophores, and the maximum emission wavelength reached the red-to-near-infrared wavelength. Most importantly, the β value in aqueous solution was significantly increased, which would be beneficial for application of the RFP dimers in two-photon fluorescence imaging and two-photon photodynamic therapy.

3.3 $^1O_2$ and $O_2^{\bullet-}$ generation evaluation in aqueous solutions of the RFP dimers

Time-dependent density functional theory (TD-DFT) was used to evaluate the differences in the generation of $^1O_2$ between the RFP dimers. As shown in ESI† (Fig. S5 and S6), the TD-DFT calculation results showed that the RFP dimers FP_2R' and FP_2R'' had small singlet–triplet energy gap (ΔE_{ST}) values of 0.10 eV and 0.11 eV, respectively, which would promote the occurrence of the intersystem crossing ISC ($S_1 \rightarrow T_3$) process, whereby $T_3 \rightarrow T_1$ would be internally converted and finally T_1 would be generated. Meanwhile, the T_1 state energies of FP_2R' and FP_2R'' were calculated to be 1.38 eV and 1.39 eV, respectively, which exceed the minimum energy of 0.98 eV required to excite molecular oxygen to form singlet oxygen.

Based on the above TD-DFT calculations results, the efficiencies of the RFP chromophore analogues for $^1O_2$ and $O_2^{\bullet-}$ production were tested in aqueous solutions. Here, 1,3-diphenylisobenzofuran (DPBF) and dihydrorhodaminutese 123 (DHR 123) were used as indicators for $^1O_2$ and $O_2^{\bullet-}$, respectively, and their mechanism of action is shown in Fig. S1 (ESI†).[36] To the best of our knowledge, there are few reports on the singlet oxygen yield (Φ_Δ) of photosensitizers in aqueous solution. Using tris(2,2′-bipyridine)dichlororuthenium(II) hexahydrate ($Ru(bpy)_3Cl_2$) as a standard reference (Φ_Δ = 0.41 in aqueous solution),[37] the RFP chromophore analogues were tested in aqueous solution (Fig. 2a and Fig. S2, ESI†). The RFP dimer FP_2R'' had the maximum singlet oxygen yield (Φ_Δ = 18%), which was 1.2-fold that of FP_2R' (Φ_Δ = 14%) and 2-fold that of FPOH (Φ_Δ = 9%). At the same time, we also tested the singlet oxygen yields of the RFP chromophore analogues in methanol, and the values for FPOH, FP_2R', and FP_2R'' were 15%, 29%, and 33%, respectively, which were higher than the singlet oxygen yield in water.

DHR 123 was used as an $O_2^{\bullet-}$ indicator to evaluate the $O_2^{\bullet-}$-production efficiency of the RFP chromophore analogues FPOH, FP_2R', and FP_2R''. As shown in Fig. 2b and Fig. S3 (ESI†), the mixtures of the aqueous solution of DHR 123 and the photosensitizers FPOH, FP_2R', and FP_2R'' produced an obvious fluorescence signal at 525 nm under light (460 nm, 23 mW cm^{-2}). The fluorescence intensity increased with the increase in irradiation time. In the mixture aqueous solution, the $O_2^{\bullet-}$ production efficiency of the photosensitizer FP_2R'' was 4.2-fold and 3.4-fold that of FPOH and FP_2R', respectively (Fig. 2d). The mechanism of $O_2^{\bullet-}$ production is shown in Fig. 2g, in which the photosensitizer FP_2R'' absorbs one photon with 496 nm and transits from its ground state (S_0) to the first singlet excited state (S_1) or the second singlet excited state (S_2). S_2 then quickly decays ($\approx$fs) to S_1 through internal conversion (IC). S_1 is also unstable with a lifetime at the ns level, and thus is inactivated either as light emission (fluorescence) or heat generated during the IC process. Meanwhile, S_1 may also undergo intersystem crossing (ISC) to form a more stable excited triplet state (T_1). T_1 exhibits a long lifetime ($\approx\mu$s) and can go through a series of photochemical reactions, such as phosphorescent emission. In addition, the singlet photosensitizer can also form free radicals in the form of a charge separation state. Subsequently, the charged radical ions will transfer electrons to the surrounding oxygen molecules, resulting in superoxide anion radicals ($O_2^{\bullet-}$). This further demonstrates that FP_2R'' has an excellent ROS production ability, which provides potential value for its application in PDT.

Electron paramagnetic resonance (EPR) spectroscopic measurements were further performed and confirmed that the RFP chromophore analogues FPOH, FP_2R', and FP_2R'' can be used as effective $^1O_2$ and $O_2^{\bullet-}$ light generators. Here, 2,2,6,6-tetramethyl-4-piperidone hydrochloride (TEMP) and 5,5-dimethyl-1-pyrroline N-oxide (DMPO) were used as $^1O_2$ and $O_2^{\bullet-}$ free radical traps, respectively. As shown in Fig. 2e and f, compared with FPOH, FP_2R' and FP_2R'' could induce strong EPR signals of TEMP after irradiation, indicating that a large amount of $^1O_2$ was produced in the mixed system. Similarly, under light irradiation (460 nm, 23 mW cm^{-2}), the EPR signal of DMPO treated with FP_2R'' under the same conditions was stronger than that of FPOH and FP_2R', indicating that more $O_2^{\bullet-}$ was generated by FP_2R''. Based on the above results, we can conclude that FPOH mainly undergoes an energy transfer process involving type II PDT to produce $^1O_2$, while the RFP dimers FP_2R' and FP_2R'' linked by alkyl chains and alkoxy chains are more inclined to produce type I $O_2^{\bullet-}$ free radicals. In summary, the RFP dimer FP_2R'' exhibited an excellent ROS ($^1O_2$ and $O_2^{\bullet-}$)-generation ability in aqueous solution, which endows it with great potential for further application in PDT.

3.4 Intracellular $^1O_2$ and $O_2^{\bullet-}$ generation under hypoxia

Due to the high $^1O_2$ and $O_2^{\bullet-}$generation efficiency and large β value of the RFP dimer FP_2R'', FP_2R'' was selected for further simulation for PDT in A-549 cells and two-photon photodynamic therapy in zebrafish. This mainly included $^1O_2$ and $O_2^{\bullet-}$ detection in normoxia (21% O_2) and hypoxic (2% O_2) environments, cell phototoxicity/dark toxicity experiments (MTT method), AO/EB double-staining experiments, and zebrafish two-photon excitation $^1O_2$ and $O_2^{\bullet-}$ imaging.

First, we evaluated the effect of the photosensitizer FP_2R'' on intracellular ROS production under normoxic (21% O_2) and hypoxic (2% O_2) environments. DCFH-DA, SOSG, and DHE were used as intracellular ROS ($^1O_2$ and $O_2^{\bullet-}$) detection kits, respectively. The mechanism of their interaction with ROS is shown in Fig. S1 (ESI†). For A-549 cells treated with the photosensitizer FP_2R'', after incubation with DCFH-DA, SOSG, and DHE for 4 h in a normoxic environment, fluorescence was generated in both the green and red channels. However, after 10 minutes of illumination, bright DCFH-DA, SOSG, and DHE fluorescence appeared in both the green and red channels. In order to better simulate the hypoxic environment of solid tumors, A-549 cells were first cultured in a hypoxic environment (2% O_2) for 8 h.

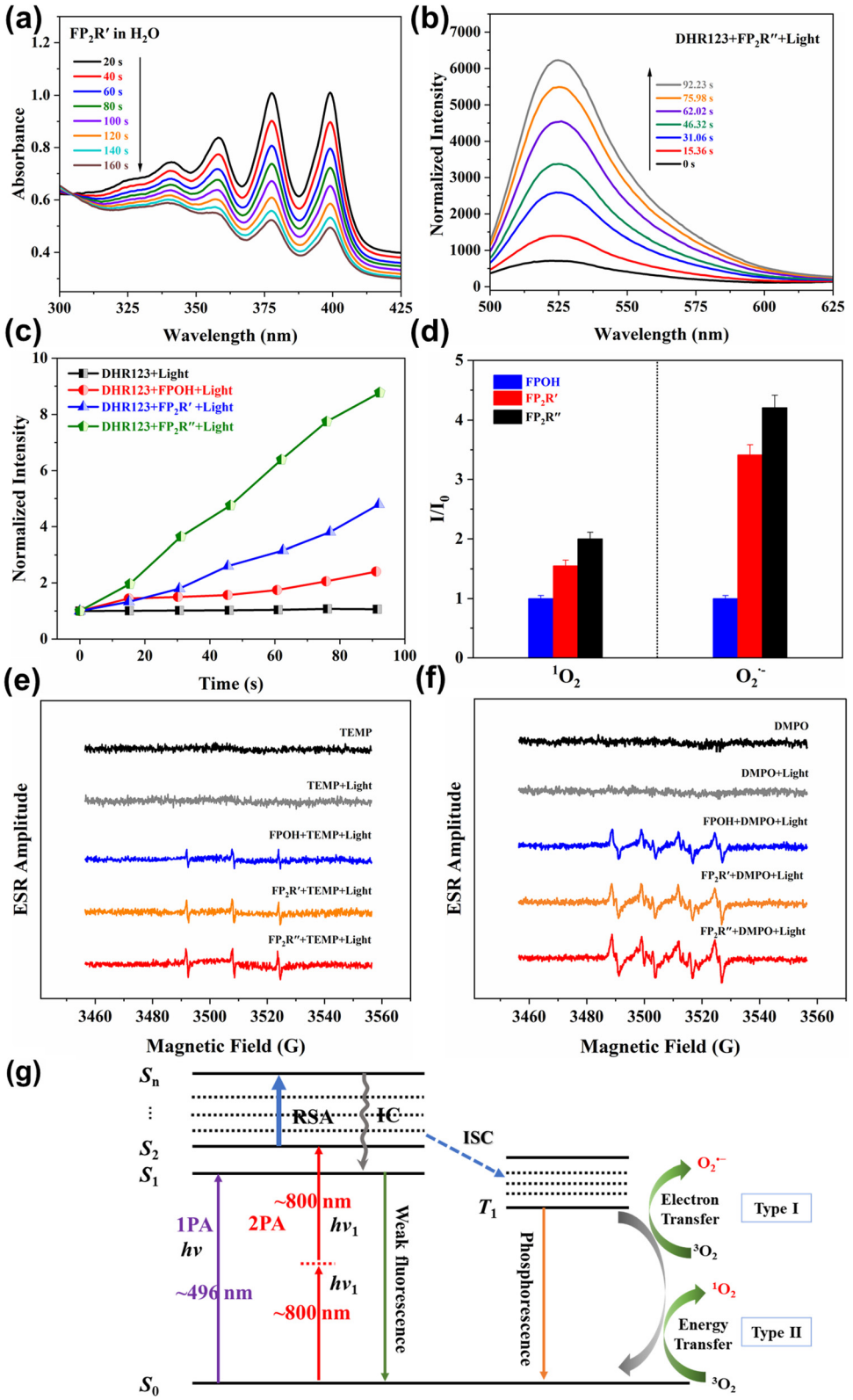

Fig. 2 (a) $^1O_2$ detection for FP_2R'' in MeOH. (b) Fluorescence spectra of DHR 123 for $O_2^{\bullet-}$ detection for FP_2R''. (c) Comparison of $O_2^{\bullet-}$ generation as a function of the irradiation time. (d) Comparison of $^1O_2$ and $O_2^{\bullet-}$ generation efficiencies for FPOH, FP_2R', and FP_2R'' under the same conditions. EPR spectra to detect $^1O_2$ (e) and $O_2^{\bullet-}$ (f) generated by FPOH, FP_2R', and FP_2R'' under irradiation (460 nm, 23 mW cm^{-2}), using DMPO as spin trapper. (g) Jablonski energy level diagram for photodynamic therapy.

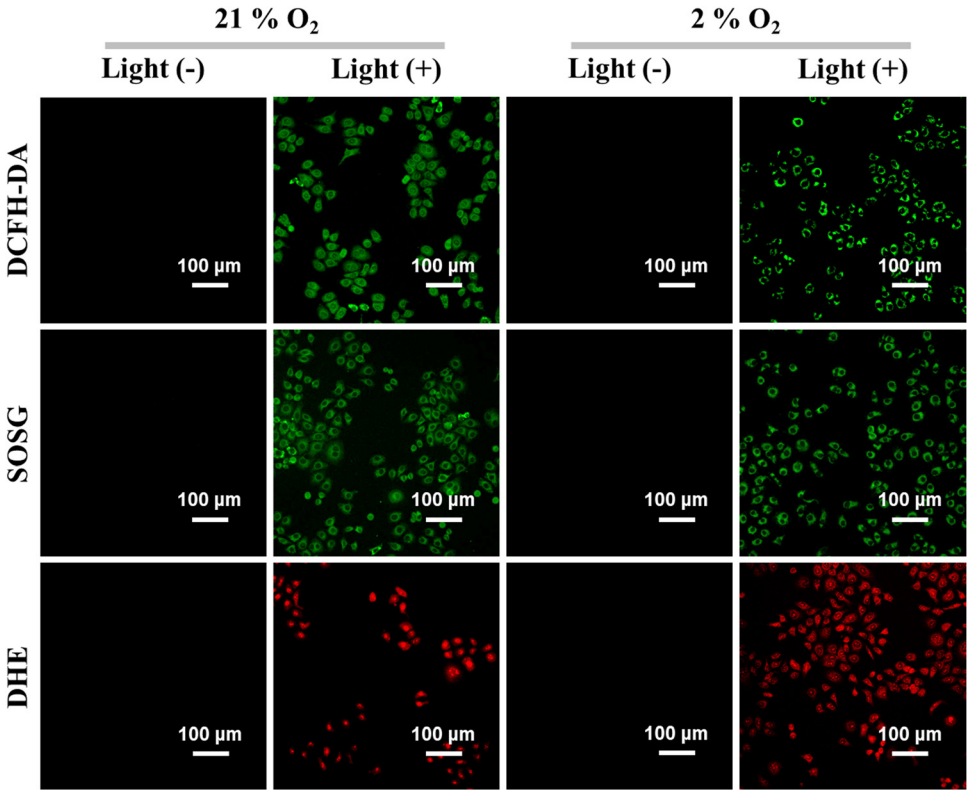

Fig. 3 ROS fluorescence imaging of the photosensitizer FP_2R'' in A-549 cells under an hypoxic microenvironment (2% O_2) and normoxia microenvironment (21% O_2).

As shown in Fig. 3, even under the hypoxic environment (2% O_2), DCFH-DA and SOSG emitted bright green fluorescence in the green channel after 10 minutes illumination. At the same time, DHE emitted satisfactory red fluorescence in the red channel. This indicates that the photosensitizer FP_2R'' could effectively produce ROS ($^1O_2$ and $O_2^{\bullet -}$) in A-549 cells after light irradiation (460 nm, 23 mW cm^{-2}). This means that the photosensitizer FP_2R'' can overcome the hypoxic environment of a tumor, which is of great significance for the design of PDT photosensitizers.

The cell phototoxicity/dark toxicity experiments of FP_2R'' in A-549 cells were performed by MTT assay using different concentrations of FP_2R'' from 1 μM to 7 μM. As shown in Fig. 4, after the 2 μM photosensitizer FP_2R'' was incubated in A-549 cells for 24 h in the dark, the A-549 cells still showed high cell viability (MTT assay > 90%). More importantly, when the oxygen concentration of the system decreased to 2%, the photosensitizer FP_2R'' still showed negligible cell dark toxicity. In addition, under 10 minutes irradiation, the maximum half inhibitory concentration (IC_{50}) values of FP_2R'' in the normoxic and hypoxic environments were 3.65 μM and 4.08 μM, respectively (Fig. S9, ESI†), indicating a high phototoxicity. These results indicate that the photosensitizer FP_2R'' showed a very small difference in cell viability between the normoxic and hypoxic environments, which is promising to overcome tumor hypoxia in PDT. The phototoxicity effect of the photosensitizer FP_2R'' on cancer cells was further visualized using the acridine orange/ethidium bromide (AO/EB) kit. The AO kit emits green fluorescence specificity for living cells, while EB can selectively bind to dead cells to emit red fluorescence. As shown in Fig. 5, under normoxic and hypoxic environments, the A-549 cells pretreated with the photosensitizer FP_2R'' only emitted strong green fluorescence in the dark, which was attributed to the AO kit's fluorescence emission, indicating that the photosensitizer FP_2R'' was non-toxic to tumor cells. However, the A-549 cells showed dual emission characteristics in the green and red channels after 10 minutes illumination (460 nm, 23 mW cm^{-2}). These results indicate that FP_2R'' could induce cancer cell death after illumination, which was consistent with the MTT experiments.

The morpholine group endows the photosensitizer FP_2R'' with excellent lysosome-targeting ability, which can greatly improve the effect of the photosensitizer in PDT. The localization of lysosomes is an important process in intracellular molecular transport and cell metabolism, which is of great significance for maintaining the normal physiological function of cells. Therefore, three commercial kits, namely Hoechst 33342, Mito-Tracker Green, and Lyso-Tracker Green, were used for A-549 cell localization studies. Here, 100 nM Lyso-Tracker Green and the photosensitizer 2 μM FP_2R'' were incubated with A-549 cells at 37 °C for 25 minutes. As shown in Fig. 6, the photosensitizer FP_2R'' and Lyso-Tracker Green emitted bright red and green fluorescence in the green and red channels, respectively, and showed an excellent overlap. The Pearson's

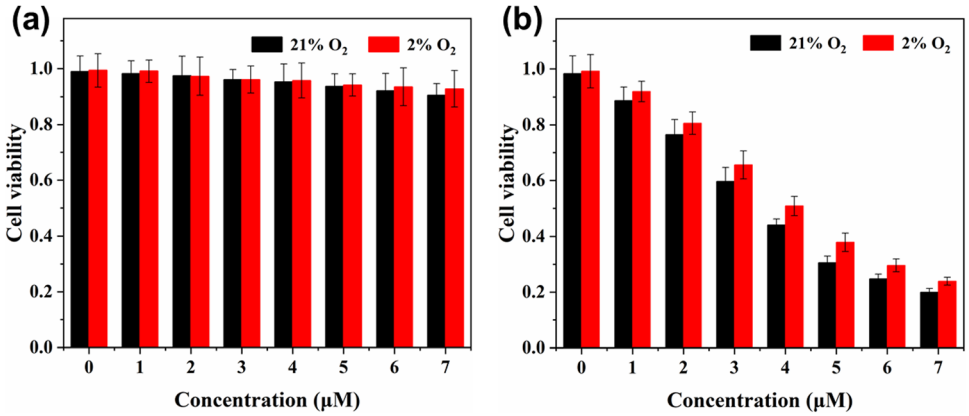

Fig. 4 Dark cytotoxicity (a) and light cytotoxicity (b) test in A-549 cells of the photosensitizer FP_2R'' (460 nm, 23 mW cm^{-2}, 10 minutes) under a hypoxic microenvironment (2% O_2) and normoxic microenvironment (21% O_2).

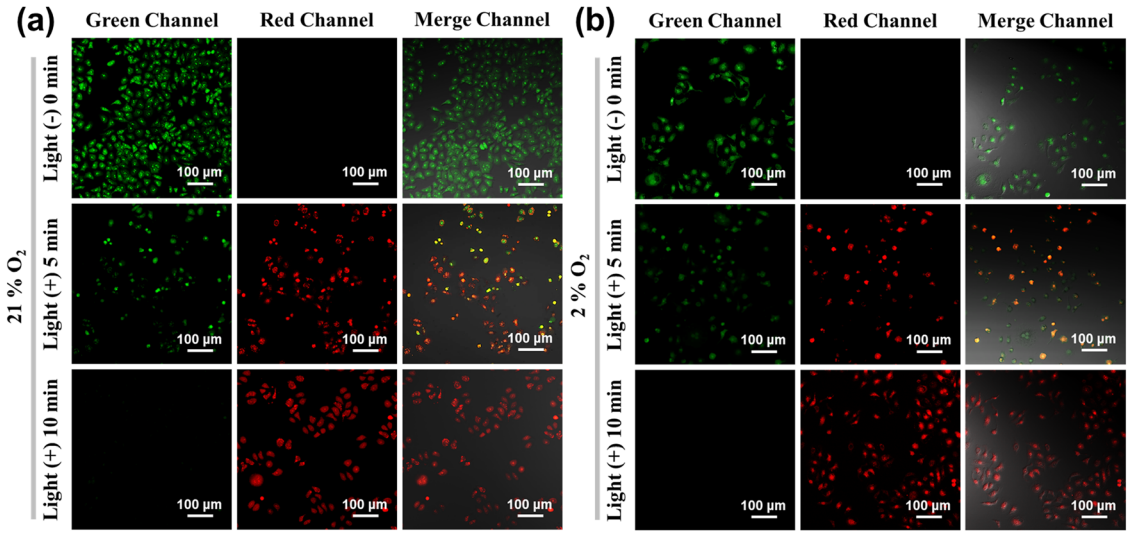

Fig. 5 AO/EB double-staining experiment for FP_2R'' in A-549 cells under a normoxic microenvironment (21% O_2) (a) and hypoxic microenvironment (2% O_2) (b). ("Light (+)" represents irradiation, "light (−)" represents without irradiation, 460 nm, 23 mW cm^{-2}, 15 minutes).

colocalization coefficient describing the correlation of the intensity distribution between the two channels was 0.94. In addition, the same experiment was performed with the photosensitizer FP_2R'' and Mito-tracker Green and Hoechst 33342. However, the red fluorescence emitted by the photosensitizer only partially overlapped with the green fluorescence emitted by Mito-tracker Green and the blue fluorescence emitted by Hoechst 33342. The Pearson's colocalization coefficients of correlation were 0.42 and 0.52, respectively. The above experimental results show that the photosensitizer FP_2R'' had an excellent lysosome-targeting ability and could specifically recognize lysosomes in A-549 cells.

3.5 Two-photon excitation photodynamic therapy evaluation in zebrafish

The two-photon absorption properties of the photosensitizer FP_2R'' endowed it with two-photon fluorescence imaging and two-photon photodynamic therapy efficiency in zebrafish. Based on the above, the effect of the photosensitizer FP_2R'' on the production of $^1O_2$ and $O_2^{\bullet-}$ in zebrafish was evaluated under 800 nm two-photon excitation. DCFH-DA, SOSG, and DHE were used as the detection kits for $^1O_2$ and $O_2^{\bullet-}$ in zebrafish, respectively. The zebrafish were incubated with the 2 μM of the photosensitizer FP_2R'' in 2 mL E3 culture medium (15 mM NaCl, 0.5 mM KCl, 1 mM $MgSO_4$, 1 mM $CaCl_2$, 0.15 mM KH_2PO_4, 0.05 mM Na_2HPO_4, 0.7 mM $NaHCO_3$; pH 7.5) for 3 h. After the aqueous solution containing the photosensitizer was removed, the zebrafish were re-incubated in an aqueous solution containing 2 μM DCFH-DA, SOSG, and DHE for 20 minutes, respectively. As shown Fig. 7a, the zebrafish treated with DCFH-DA and SOSG showed no fluorescence in the green channel without two-photon laser scanning. After 800 nm two-photon excitation scanning, the zebrafish emitted bright DCFH-DA and SOSG green fluorescence in the green channel. It was thus shown that the photosensitizer FP_2R'' could effectively produce $^1O_2$ under two-photon excitation. In addition,

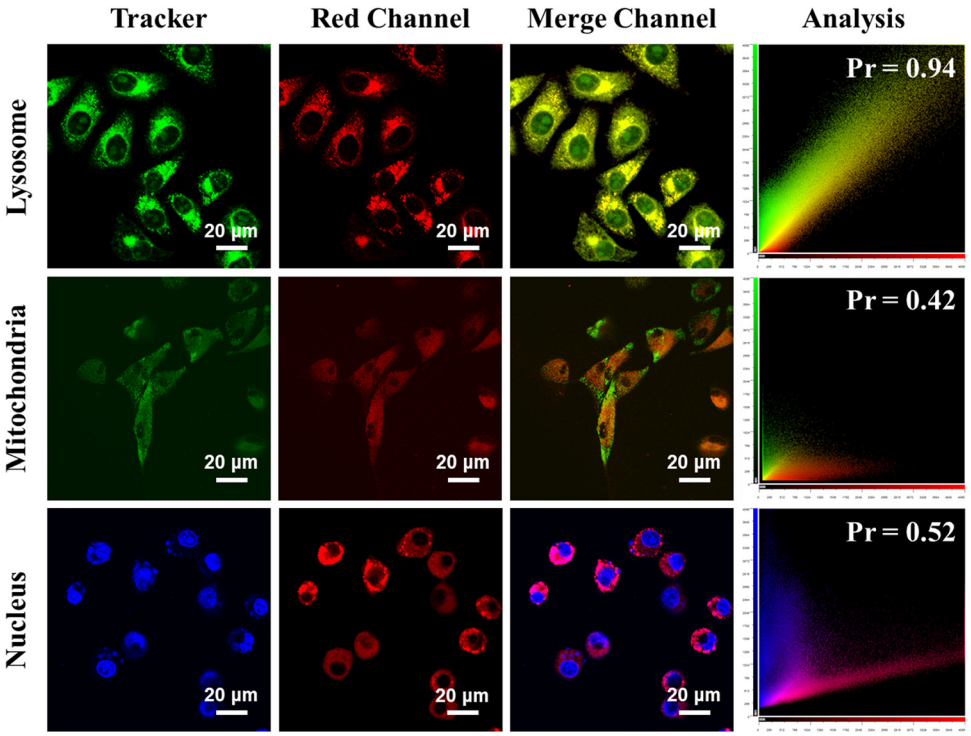

Fig. 6 Confocal fluorescence images of the photosensitizer FP_2R'' colocalization of organelles in A-549 cells. Scale bars: 20 μm.

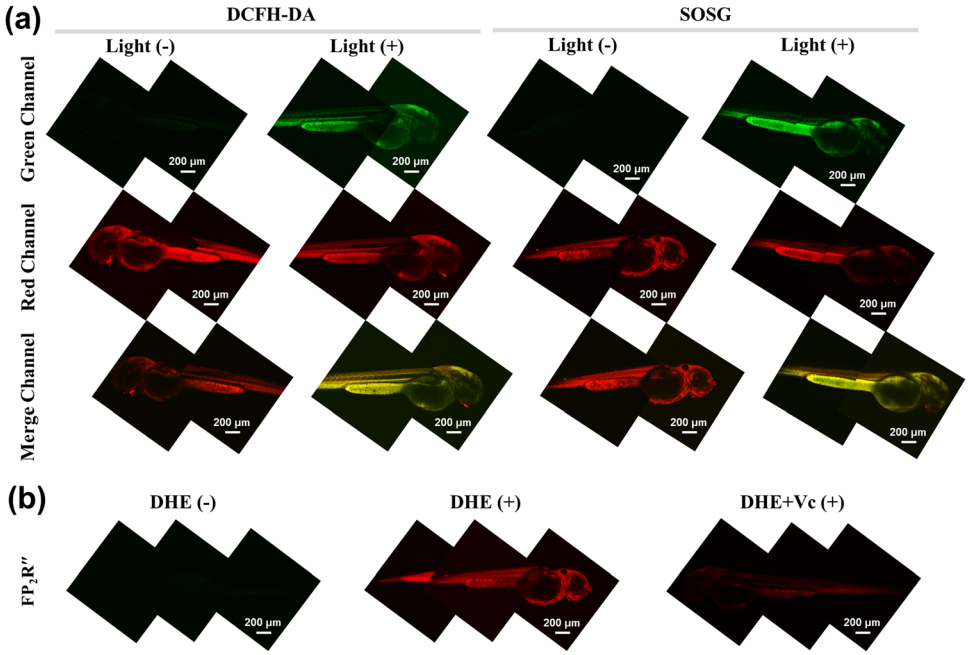

Fig. 7 Detection of ROS in two-photon fluorescence imaging in zebrafish using DCFH-DA, SOSG, and DHE with the photosensitizer FP_2R''.

when the zebrafish treated with DHE were scanned with an 800 nm laser, DHE was oxidized by the $O_2^{\bullet-}$ generated by FP_2R'' and emitted bright red fluorescence in the red channel. At the same time, the zebrafish treated with vitamin C (VC) by two-photon laser scanning only emitted weak red fluorescence. It was thus proved that the photosensitizer FP_2R'' could effectively produce $O_2^{\bullet-}$ in zebrafish under two-photon excitation. The above experiments further proved that FP_2R'' can be used as a two-photon photosensitizer and it could be expected to be used in the treatment of two-photon-activated cancer tumor cells.

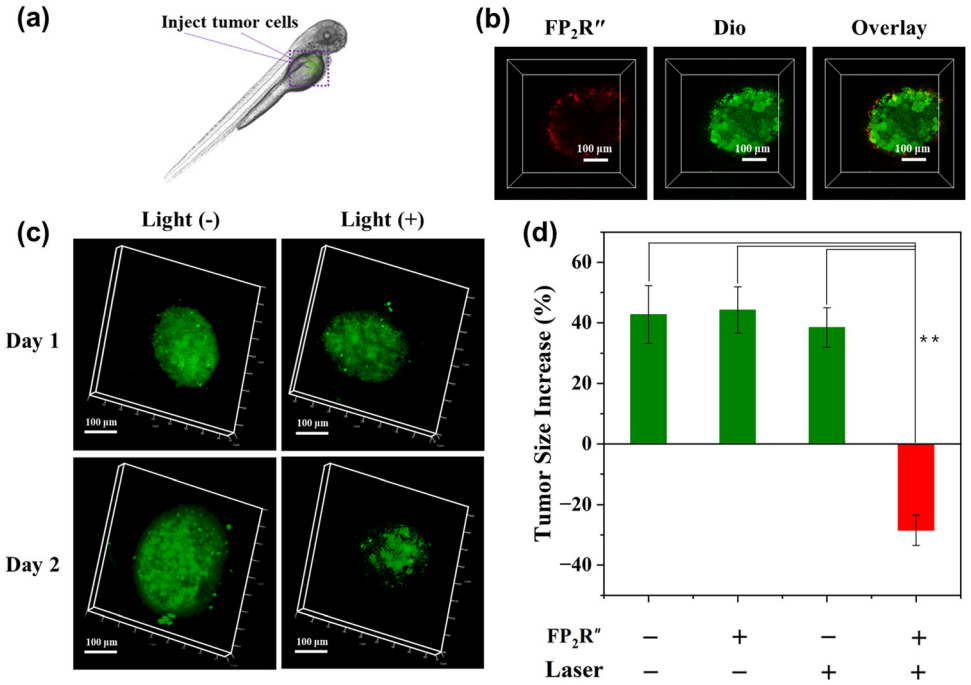

Fig. 8 (a) Schematic illustration of the *in vivo* two-photon photodynamic therapy of FP_2R'' in the zebrafish liver tumor model; (b) two-photon fluorescence images of FP_2R'' (FP_2R'', red) distributed in the zebrafish liver tumor (Dio, green). Excitation: 800 nm; emission: 635–675 nm (red) and 510–535 nm (green); (c) changes in the size of the zebrafish liver tumors in the control group before (day 1) and after (day 2) two-photon photodynamic therapy; (d) relative increase in the tumor sizes of the zebrafish after treatment under different conditions (%) (**$p < 0.01$).

3.6 Two-photon photodynamic therapy for zebrafish as liver tumor treatment

Due to the relatively small size of the zebrafish liver tumor, it is suitable for two-photon microscopy for *in vivo* PDT.[38–40] Consequently, the photosensitizer FP_2R'' was injected intravenously into the zebrafish, and its distribution in liver tumors was evaluated by two-photon fluorescence imaging. The detailed protocol for preparation of the liver tumor model can be found in the experimental section 2.9. As shown in Fig. 8, the red fluorescence of FP_2R'' and the green fluorescence of the zebrafish liver tumors could be clearly observed under 800 nm two-photon excitation. The two-photon fluorescence image shows that the photosensitizer FP_2R'' had a good positioning effect in the green liver tissue, revealing its good aggregation effect in zebrafish liver tumors, which is conducive to two-photon photodynamic therapy in zebrafish. After 20 minutes two-photon laser irradiation (800 nm, 3 mW) for two consecutive days, the tumor size changes before and after the two-photon photodynamic therapy were measured by confocal microscopy. As shown in Fig. 8d, the size of the liver tumor after the two-photon photodynamic therapy treatment showed a decrease of about 28%, while the size of the tumor in the control group was increased by 38–42%. These results demonstrate that FP_2R'' had an excellent effect on PDT in zebrafish under two-photon excitation.

Compared with traditional PDT, two-photon activated PDT has multiple advantages, such as reducing light-induced damage, improving the imaging resolution of turbid samples, and most importantly, an extended PDT window for deep-tissue processing. The RFP dimer was applied to the tumor zebrafish model in two-photon PDT experiments, and the two-photon PDT experiments showed that FP_2R'' achieved impressive tumor suppression and good biosafety under two-photon laser radiation.

The two-photon absorption cross-section testing and simulated PDT experiments in zebrafish indicated that the alkoxy and alkyl chain links significantly improved the RFP dimers aqueous solubility, the $^1O_2$ and $O_2^{\bullet-}$ yields, and the two-photon absorption property. It is worth mentioning that the RFP dimer FP_2R'' could not only produce $^1O_2/O_2^{\bullet-}$ in hypoxic environments in the simulated PDT experiments, but could also achieve the inhibition of the growth of tumor cells in zebrafish under two-photon excitation PDT. This provides important value for the development of hypoxia two-photon photosensitizers.

4. Conclusions

In summary, two water-soluble RFP dimers (FP_2R' and FP_2R'') were synthetized by linking two phenothiazine-based RFP chromophore analogues through alkyl chains and alkoxy chains for hypoxia two-photon PDT. The modification of the water-soluble RFP dimers endowed them with an aqueous solubility of 3.5 mM, emission wavelength of 677 nm, and β of 2.1×10^{-11} cm W^{-1}. In addition, the heavy-atom-free structural design endowed FP_2R'' with a smaller single-triplet (ΔE_{ST} = 0.11 eV), which was conducive to the occurrence of intersystem crossing between $S_1 \rightarrow T_3$ states and promoted the production of ROS. In biological experiments, the photosensitizer FP_2R'' demonstrated good biocompatibility and could be

quickly taken in by A-549 cells. It is worth mentioning that under an hypoxic environment, the RFP dimer FP_2R'' exhibited high phototoxicity, with an IC_{50} value of 4.08 μM, indicating that FP_2R'' has excellent anti-hypoxia abilities. In addition, the photosensitizer FP_2R'' demonstrated a precise lysosome-targeting ability (Pearson's colocalization coefficient: 0.94), which could guide the photosensitizers aggregation in the lysosomes of tumor cells and effectively improve its PDT effect. Under 800 nm two-photon excitation, the photosensitizer FP_2R'' could effectively generate $^1O_2$ and $O_2^{\bullet-}$ in zebrafish, resulting in bright and clear two-photon fluorescence images. In addition, FP_2R'' achieved the inhibition of tumor cells growth in zebrafish under two-photon excitation PDT, which provides potential value for the treatment of hypoxic tumors. Through this work, we envision FP_2R'' as an efficient hypoxia two-photon photosensitizer, and this design strategy will provide an important perspective for the future development of effective type I two-photon photosensitizers.

Authors sontributions

Wan Feng: synthesis and testing of compounds, and writing – original draft. Ying Qian: fund acquisition, concept formation, writing – review, and editing.

Conflicts of interest

There are no conflicts to declare.

Acknowledgements

This work was financially supported by the Fundamental Research Funds for the National Natural Science Foundation of China (No. 62075039).

References

1 D. K. Joshi, F. Betancourt, M. Pilkington and H. B. Yan, *J. Photochem. Photobiol., A*, 2023, **442**, 114770.
2 B. Dorota, W. Paweł, D. Klaudia and A. David, *Brain Sci.*, 2023, **13**, 1299.
3 L. Peng, W. Chen, H. Hou, M. Tian, F. Song, W. Zheng and X. Peng, *Dyes Pigm.*, 2023, **217**, 111426.
4 J. Wen, Y. Luo, H. Gao, L. Zhang, X. Wang, J. Huang, T. Shang, D. Zhou, D. Wang, Z. Wang, P. Li and Z. Wang, *J. Nanobiotechnol.*, 2021, **19**, 440.
5 B. F. Hohlfeld, D. Steen, G. D. Wieland, K. Achazi, N. Kulak, R. Haaga and A. Wiehe, *Org. Biomol. Chem.*, 2023, **21**, 3105.
6 F. Setaro, J. W. H. Wennink, P. I. Mäkinen, L. Holappa, P. N. Trohopoulos, S. Ylä-Herttuala, C. F. Nostrum, A. Escosura and T. Torres, *J. Mater. Chem. B*, 2020, **8**, 282.
7 Y. Xu, C. Teng, H. Dang, D. Yin and L. Yan, *Talanta*, 2024, **266**, 124948.
8 S. Tang, R. Yang, Y. Gao, L. Zhu, S. Zheng and X. Zan, *ACS Macro Lett.*, 2023, **12**, 639–645.
9 J. S. Cisneros, C. Y. Chain, M. B. Aiello, J. Parisi, D. C. Castrogiovanni, G. N. Bosio, D. O. Mártire and M. E. Vela, *ACS Omega*, 2021, **6**, 12567–12576.
10 S. Moghassemi, A. Dadashzadeh, R. B. Azevedo and C. A. Amorim, *J. Controlled Release*, 2022, **351**, 164–173.
11 B. Yang, Y. Chen and J. Shi, *Chem. Rev.*, 2019, **119**, 4881–4985.
12 Z. Chen, C. T. Vong, C. Gao, S. Chen, X. Wu, S. Wang and Y. Wang, *Mol. Pharmaceutics*, 2020, **17**, 2260–2274.
13 Y. Li, H. Bai, H. Wang, Y. Shen, G. Tang and Y. Ping, *Nanoscale*, 2018, **10**, 203.
14 T. Lyu, S. H. Sohn, R. Jimenez and T. Joo, *J. Phys. Chem. B*, 2022, **126**(12), 2337–2344.
15 S. A. Boulanger, C. Chen, I. N. Myasnyanko, M. S. Baranov and C. Fang, *J. Phys. Chem. B*, 2022, **126**, 5081–5093.
16 L. Tang and C. Fang, *J. Phys. Chem. B*, 2021, **125**, 13610–13623.
17 M. Zimmer, *Chem. Soc. Rev.*, 2009, **38**, 2823–2832.
18 J. Dong, K. M. Solntsev, O. Poizat and L. M. Tolbert, *J. Am. Chem. Soc.*, 2007, **129**, 10084–10085.
19 H. Chen, L. Liu, K. Qian, H. Liu, Z. Wang, F. Gao, C. Qu, W. Dai, D. Lin, K. Chen, H. Liu and Z. Cheng, *Sci. Adv.*, 2022, **8**, eabo3289.
20 H. Leng, Y. Wang, J. Wang, H. Sun, A. Sun, M. Pistolozzi, L. Zhang and J. Yan, *Anal. Chem.*, 2022, **94**, 1999–2006.
21 X. Liu, L. Yang, X. Li, L. Zhao, S. Wang, Z.-H. Lu, J. Ding and L. Wang, *Angew. Chem., Int. Ed.*, 2021, **60**, 2455–2463.
22 B. Shen, W. Zhu, X. Zhi and Y. Qian, *Talanta*, 2020, **208**, 120461.
23 Y. Liu, C. H. Wolstenholme, G. C. Carter, H. Liu, H. Hu, L. S. Grainger, K. Miao, M. Fares, C. A. Hoelzel, H. P. Yennawar, G. Ning, M. Du, L. Bai, X. Li and X. Zhang, *J. Am. Chem. Soc.*, 2018, **140**, 7381–7384.
24 C. M. Lemon and M. A. Marletta, *Inorg. Chem.*, 2021, **60**, 2716–2729.
25 M. Hirano, *Nat. Biotechnol.*, 2022, **40**, 1132–1142.
26 A. Dance, *Nature*, 2021, **596**, 152–153.
27 M. Wang, Y. Da and Y. Tian, *Chem. Soc. Rev.*, 2023, **52**, 1189.
28 Z. Qu, J. Fang, Y.-X. Wang, Y. Sun, Y. Liu, W.-H. Wu and W.-B. Zhang, *Nat. Commun.*, 2023, **14**, 3480.
29 R. Jöhr, M. S. Bauer, L. C. Schendel, C. Kluger and H. E. Gaub, *Nano Lett.*, 2019, **19**, 3176–3181.
30 W. Li, W. Feng, B. Liu and Y. Qian, *J. Photochem. Photobiol., A*, 2023, **445**, 115045.
31 W. Xiang, B. Liu and Y. Qian, *Dyes Pigm.*, 2022, **205**, 110524.
32 X. Zhi and Y. Qian, *Talanta*, 2021, **222**, 121503.
33 W. Feng, W. Li and Y. Qian, *Dyes Pigm.*, 2023, **220**, 111714.
34 X. Zhao, F. Zhou, Q. Liu, Q.-F. Chen, J.-Y. Yang, W.-H. Zhang, Y.-L. Song and J.-P. Lang, *Inorg. Chem.*, 2016, **55**, 1861–1871.
35 R.-J. Niu, W.-F. Zhou, Y. Liu, J.-Y. Yang, W.-H. Zhang, J.-P. Lang and D. J. Young, *Chem. Commun.*, 2019, **55**, 4873.
36 Y.-F. Xiao, W.-C. Chen, J.-X. Chen, G. Lu, S. Tian, X. Cui, Z. Zhang, H. Chen, Y. Wan, S. Li and C.-S. Lee, *ACS Appl. Mater. Interfaces*, 2022, **14**, 5112–5121.
37 C. Tanielian, C. Wolff and M. Esch, *J. Phys. Chem.*, 1996, **100**, 6555–6560.
38 G. vLieschke and P. Currie, *Nat. Rev. Genet.*, 2007, **8**, 353–367.
39 A. T. Nguyen, A. Emelyanov, C. H. V. Koh, J. M. Spitsbergen, S. Parinov and Z. Gong, *Dis. Models Mech.*, 2012, **5**, 63–72.
40 R. White, K. Rose and L. Zon, *Nat. Rev. Cancer*, 2013, **13**, 624–636.

